The FITME Project: Personalized Obesity Profiling by Integrating 4D Body Scanning, Functional Analysis, Infrared Thermography, Medical Imaging, and Biological Indicators

Nerea CILLERUELO*, Eduardo PARRILLA*, Alfredo BALLESTER*,
Consuelo LATORRE*, Ainhoa RODRIGUEZ DE LUIS*, Alvaro HUGUET*
Instituto de Biomecanica de Valencia (IBV), Universitat Politecnica de Valencia (UPV), Valencia, Spain

https://doi.org/10.15221/yy.nn

Abstract

Traditional obesity assessment methods, reliant on simple indicators like body mass index (BMI), provide limited insight into individualized obesity risk profiles. The FITME project addresses this limitation by developing a multi-sensor, radiation-free framework for precision obesity profiling, capturing inter-individual variability. At its core, the Human Analysis Laboratory (HAL) integrates synchronized 3D/4D optical body scanning (MOVE4D), infrared thermography (IRT), and markerless motion analysis to precisely capture morphology, thermoregulation, and functional performance. These external-body measurements are validated against reference standards for body composition (including medical imaging DXA/CT), and contextualized by a detailed set of Supplemental Biological Indicators (S-BIs), including clinical biochemistry and gut microbiota profiling. The integration of these domains produces anatomically registered 3D models enriched with cross-validated data sources. The pipeline generates Obesity Indicators (OIs) derived from the fusion of these domains. The ultimate aim is to train and validate AI predictive models using OIs to accurately estimate body composition, shape, muscular function, and Metabolic Syndrome (MetS) risk. A representative case study illustrates the methodology.

Keywords: 3D/4D body scanning, infrared thermography, markerless motion analysis, metabolic syndrome (MetS), radiation-free.

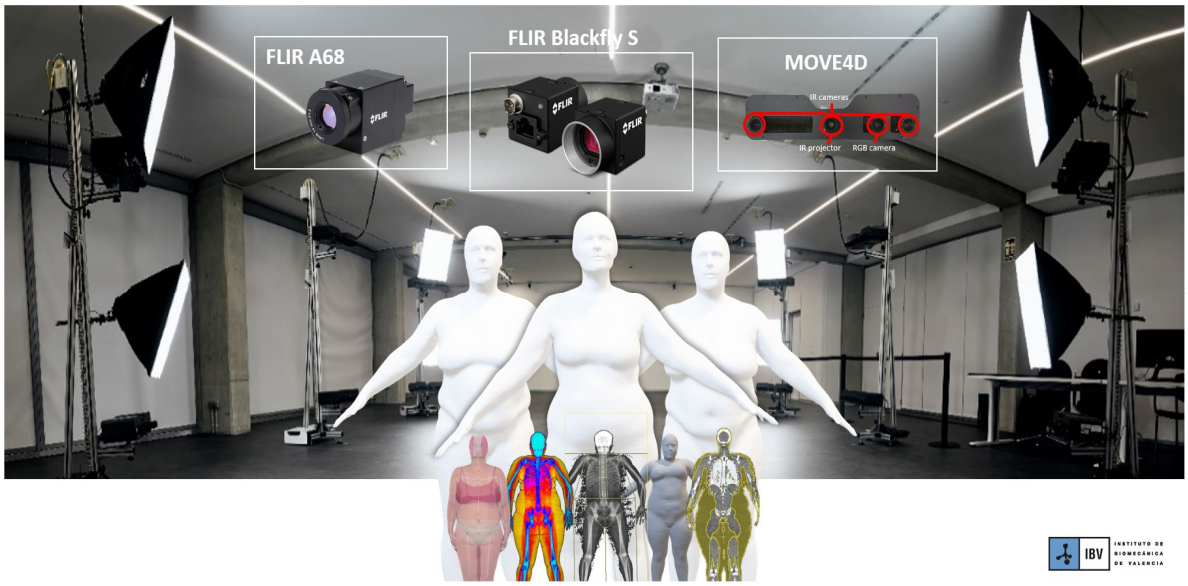

Figure 1: Overview of the HAL multi-sensor system.

* *Corresponding authors: nerea.cilleruelo@ibv.org, eduardo.parrilla@ibv.org, alfredo.ballester@ibv.org, consuelo.latorre@ibv.org, ainhoa.rodriguez@ibv.org, alvaro.huguet@ibv.org – www.ibv.org*

†*Acknowledgment: This work was conducted within the FITME project, funded by the Agencia Valenciana de la Innovacion (AVI) and co-financed by the European Regional Development Fund (ERDF), S3-CV 2021–2027 strategy (reference INNEST/2024/275). The authors also thank the FITME consortium partners: ECG Medica S.L. (ASCIRES), SABARTECH S.L., and the Fundacion para la Investigacion del Hospital Clinico de la Comunidad Valencia (INCLIVA) along with the technical staff and study participants.*

1. Introduction

Obesity is a chronic, multifactorial, and complex disease characterized not only by excess body weight but also by the distribution and composition of fat and lean tissues [1–3]. Beyond the classical energy imbalance be- tween intake and expenditure, obesity results from the interaction of multiple determinants, including genetic, metabolic, behavioral, and psychosocial factors [1, 4]. This condition is closely associated with an elevated risk of cardiovascular disease, type 2 diabetes, certain cancers, and a wide spectrum of behavioral and physical complications [5, 6]. Among the various obesity phenotypes, visceral adiposity and central fat accumulation exhibit the strongest associations with adverse metabolic outcomes, particularly Metabolic Syndrome (MetS) and cardiovascular disease [7].

Currently, more than one billion people worldwide are affected by obesity, with prevalence rising rapidly among children and adolescents. The World Health Organization (WHO) classifies obesity as a global pandemic that demands coordinated public health strategies [3, 9, 10]. Despite this alarming prevalence, obesity assessment remains largely dependent on BMI due to its simplicity and applicability at the population level. However, BMI provides only a partial representation of the body: as a simple ratio of weight to height, it fails to distinguish fat from lean tissue or reflect the anatomical distribution or metabolic activity of adipose tissue. Individuals with identical BMI values may differ substantially in visceral adiposity, muscularity, and cardiometabolic risk [1]. These limitations underscore the need for more comprehensive and individualized approaches integrating multiple physiological dimensions to characterize obesity beyond BMI.

To address these shortcomings, the FITME project was conceived to develop a novel, radiation-free framework capable of accurately estimating body composition, body shape, muscular function, and MetS risk in individuals with obesity. Recent advances in three-dimensional optical imaging have demonstrated the feasibility of precise, non-invasive analysis of body shape and composition, reinforcing its potential as a radiation-free alternative to conventional gold standards.

Building upon these advancements, FITME extends the concept of radiation-free obesity profiling by integrating synchronized 4D body scanning, infrared thermography (IRT), and markerless motion analysis. Crucially, these external measurements are combined with medical imaging and a Supplemental Biological Indicators (S-BIs), to enable a unified and personalized understanding of obesity variability. The specific goal of this study is to validate radiation-free methodologies by comparing external multi-source measurements against internal gold-standard references (DXA/CT). From these radiation-free technologies, a set of Obesity Indicators (OIs) is derived and integrated into a dataset that constitutes the foundation for the development and validation of next-generation AI-driven predictive models aimed at precision, radiation-free assessment of body composition and metabolic health.

2. Theoretical Background

Obesity is strongly linked to Metabolic Syndrome (MetS), a cluster of clinical abnormalities that reflect overnutrition, sedentary lifestyle, and excess adiposity [12, 13]. MetS is typically diagnosed when three or more unfavorable measures are present, including increased waist circumference (WC), elevated plasma triglycerides, high blood pressure (BP), impaired fasting glucose, and reduced high-density lipoprotein (HDL) cholesterol [8, 13]. These markers correspond to metabolic disturbances that elevate the risk of cardiovascular and other chronic dis- eases [11, 12]. The cumulative presence of MetS components substantially increases both clinical and economic burden, with healthcare costs rising by approximately 24% per additional risk factor [14]. This highlights the importance of early detection to mitigate long-term health risks [12, 13].

Traditional anthropometric indicators, such as BMI or waist circumference, offer limited insight into interindividual variability in fat distribution, metabolic health, and functional capacity [16, 17]. The WHO defines obesity as “abnormal or excessive fat accumulation that presents a risk to health,” using BMI ≥ 30 kg/m² as the diagnostic threshold in adults [3]. However, BMI, while globally standardized, cannot fully capture body composition or risk heterogeneity [1, 4]. Although higher BMI values generally correlate with MetS risk across normal-weight and overweight adults [7], the metric often misclassifies muscular individuals or those with normal BMI but excess fat, leading to inaccurate estimations of their true MetS risk [15]. The type and distribution of adipose tissue are critical determinants of MetS: visceral fat surrounding internal organs poses the greatest cardiometabolic risk, even in normal-BMI individuals, while subcutaneous fat tends to be metabolically less harmful [7].

Traditional techniques (e.g., skinfolds, DXA, MRI, or questionnaires) address these parameters separately and often face challenges related to accuracy, invasiveness, or cost [2, 18]. This highlights the need for integrated, radiation-free approaches for personalized obesity evaluation [4, 19]. Advanced imaging modalities such as DXA and CT provide detailed body composition measures, but their reliance on ionizing radiation limits their feasibility for routine assessments. Modern approaches increasingly rely on advanced technologies. In particular, the combination of 3D/4D body scanning and motion capture offers new opportunities for in vivo obesity profiling, addressing the limitations of conventional methods [20]. Studies that merge 3D surface scans with medical imag- ing demonstrate strong correlations between external body shape and internal body composition [21, 22]. While CT remains the gold standard for assessing visceral adiposity [5], emerging methods such as IRT and multi-omics profiling offer radiation-free insights into metabolic and molecular diversity [4, 23].

Unlike manual tape measurements or traditional imaging involving ionizing radiation, high cost, and limited accessibility, 3D optical scanning offers an objective, safe, and repeatable method for assessing body morphology. Notably, 3D-derived body shape features have been shown to enhance prediction of MetS and body com- position compared with BMI alone [21, 24]. Although marker-based motion analysis offers high accuracy, it is time-consuming and intrusive, requiring markers, sensors, and operator expertise. Conversely, markerless and contactless technologies streamline the process by capturing body morphology (3D shape), dynamic motion (4D), and surface temperature maps (IRT) in a single integrated framework. These systems preserve the participant's natural posture and movement, enhance comfort, reduce preparation time, and lower costs, improving feasibility for both research and clinical applications [25].

Skin temperature patterns, reflecting blood perfusion and metabolic activity, can indicate vascular dysfunction or altered thermogenesis. Conditions such as inflammation or insulin resistance produce distinct thermal signatures on the skin surface [6]. For instance, individuals with MetS often show higher facial and hand temperatures, whereas obese adults exhibit cooler abdominal regions due to the insulating effect of subcutaneous fat [26]. Consequently, IRT emerges as a valuable, radiation-free tool for assessing metabolic dysfunction and thermoregulatory imbalance.

3. Materials and Methods

3.1. Study Design and Participants

A prospective study was designed to recruit 100 adults (sex-balanced, 18–70 years) classified as overweight (BMI 25–29.9 kg/m^2) or obese (BMI ≥30 kg/m^2). One representative case is analyzed in detail in this paper. All participants provide written informed consent prior to enrollment.

All measurements are conducted within a three-week window, with approximately one week between sessions to maintain stable physiological and morphological conditions. The study protocol received approval from the Research Ethics Committee for Medicines (CEIm) of the University Clinical Hospital of Valencia. Data collection is being carried out between May 2025 and July 2026, and all measurements are performed by trained technicians under standardized procedures to ensure accuracy, reliability and reproducibility.

3.2. Data collection

The FITME protocol is defined by the integration of a suite of complementary state-of-the-art assessment tools. These modalities are grouped into three main data domains that feed into the AI modeling and validation pipeline (Figure 2):

- **Body Composition Reference Standards:** These represent the gold-standard methods for quantifying internal body composition and fat distribution. Dual-energy X-ray absorptiometry (DXA) was used to measure total and regional body composition. Computed tomography (CT) was employed for precise quantification of visceral adipose tissue (VAT) and subcutaneous adipose tissue (SAT). Bioimpedance analysis (BIA) provided additional estimations of body composition and hydration status.
- **External Morphofunctional Domain:** These radiation-free systems, implemented within the HAL, cap- ture external body morphology, function, and physiology, using synchronized: 3D/4D body scanning (for anthropometry, geometry, and motion); Infrared thermography (IRT) (for surface temperature and physio- logical response); and markerless motion analysis complemented by dynamometry (to quantify gait, posture, and muscle strength).

- **Supplemental Biological Indicators (S-BIs):** A comprehensive collection of clinical biomarkers (e.g., lipid profile, hormones, inflammatory markers) and gut microbiota profiling. These serve as molecular endpoints, providing essential biological context to phenotypes derived from external 4D/IR data.

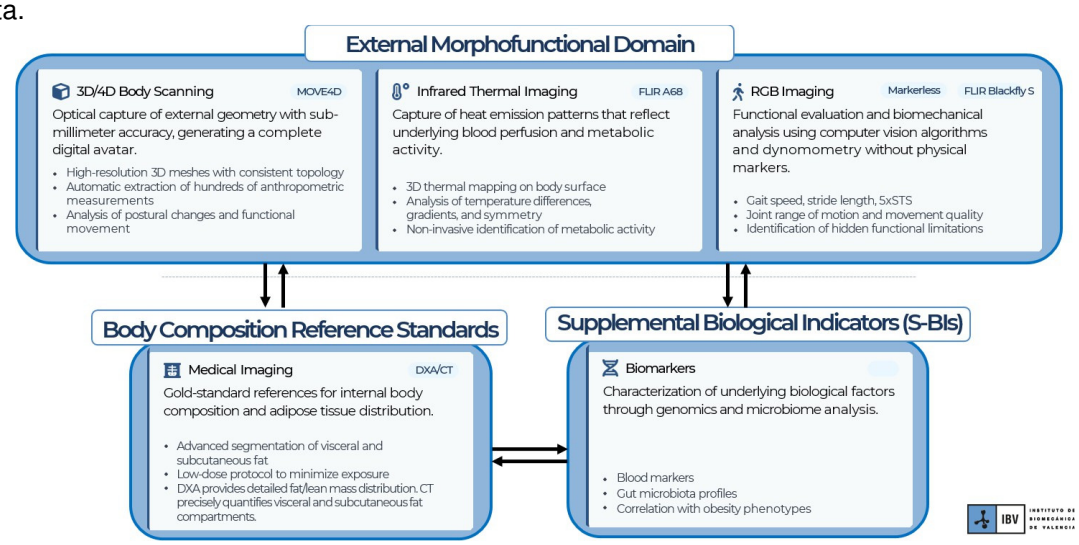

Figure 2: Overview of the main FITME data sources: (i) body composition reference standards (DXA, CT, BIA), (ii) external morphofunctional domain (3D/4D scanning, IRT, markerless motion, dynamometry), and (iii) S-BIs.

3.2.1. HAL Multi-sensor System

The Human Analysis Laboratory (HAL) integrates three synchronized core technologies within a unified infrastructure: (i) the MOVE4D dynamic body scanner, (ii) a multi-camera RGB array, and (iii) a thermal imaging array (Figure 1).

- **3D/4D Body Scanning (MOVE4D, 3D Avatar Body App):** The MOVE4D system captures external body geometry with sub-millimeter accuracy, generating high-resolution 3D meshes and dynamic 4D sequences with consistent topology over time [28]. Static scans (3D Avatar Body App) generate digital avatars for anthropometric assessment, while dynamic 4D sequences record posture, shape and motion, enabling ex- traction of hundreds of metrics during movement. Compared with CT or MRI, optical scanning is fast, safe, and repeatable [29], and has shown predictive value for MetS risk beyond BMI [21].
  The system includes 16 modular sensor units, each combining IR cameras, an IR projector, and an RGB camera, reconstructing high-density 3D point clouds at ∼1 mm resolution. Ultra-short exposures (∼1 ms) minimize motion blur, with real-time processing at ∼15 FPS and capacity up to 178 FPS for fast-motion.
- **Infrared Thermography (IRT) Imaging:** High-definition thermographic cameras capture skin temperature maps that reflect underlying blood perfusion and metabolic activity [6]. When integrated with 4D scans, these data enable projection of regional hot and cold spots, quantification of thermal gradients, and bilateral symmetry analysis, providing radiation-free biomarkers of inflammation, adipose tissue activity and vascular dysfunction [26]. IRT is fast, contact-free, radiation-free, and scalable, reinforcing its potential for large-scale metabolic screening.
  The setup comprises eight FLIR A68 LWIR cameras (8–14 μm), delivering 16-bit radiometric output at 640 × 480 px and 30 FPS. The cameras are distributed throughout the capture volume to optimize coverage and minimize reflections. GigE networking and PTP synchronization in combination with external sync signal support, ensure precise temporal alignment with 3D and RGB streams.
- **Markerless Biomechanical Analysis:** RGB cameras capture functional tasks without markers or suits. Computer vision algorithms extract joint kinematics to compute quantitative metrics such as gait speed, stride length, angular velocity, or range of motion. This approach provides objective measures of functional capacity and mobility, enabling correlation of body composition with biomechanical performance and detection of obesity-related impairments (e.g., reduced mobility, musculoskeletal stress).
  A set of 16 industrial RGB cameras (FLIR Blackfly S) provide overlapping fields of view. Each unit captures images at a 1440 × 1080 px and up to 74 FPS. Global shutters and synchronized signals guarantees time- aligned acquisition across modalities.

Data from these modalities are fused into unified 3D representations, where each surface vertex encodes geometric, color, and thermal information (Figure 3). This spatiotemporal synchronization allows simultaneous analysis of shape, motion, and thermographic features within the same anatomical context, under controlled environmental conditions.

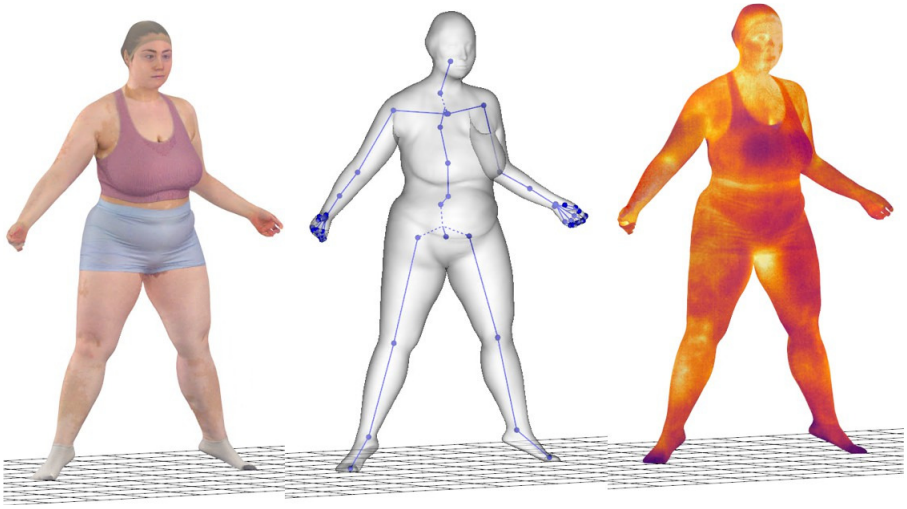

Figure 3: Multi-sensor fusion from the HAL pipeline: synchronized 3D, RGB, and thermal data integrated into a single spatiotemporally aligned model.

Subsystem Technical Specifications are summarized in Table 1, describing sensor configurations, resolution, frame rates, and synchronization features across subsystems. This setup enables the acquisition of dense 3D point clouds (~4M points/frame), high-resolution video, and thermal maps in strict temporal and spatial coherence. All cameras undergo geometric calibration, including the three cameras in each MOVE4D unit, and thermal sensors are additionally radiometrically calibrated and thermally stabilized before acquisition. The HAL operates within a controlled 2 × 3 × 3 m capture volume, minimizing occlusions and ensuring total coverage.

Table 1: Subsystem configurations in the HAL multi-sensor capture system.

Subsystem	Components (Count)	Resolution & Frame Rate	Notable Features
MOVE4D capture system	16 IR sensor units (2 IR cameras + 1 IR projector + 1 RGB camera each)	~1 mm resolution; up to 90 FPS (full-res) or 178 FPS (reduced); 15 FPS real-time processing	4M points/frame; 1 ms exposure to freeze motion; sync in/out, trigger in
RGB multi-camera array	16 FLIR Blackfly S (BFS-PGE-1652C-CS)	1440 × 1080 px at 74 FPS	GigE Vision; global shutter; 360° arrangement; overlapping fields of view; GigE interface; sync in/out, trigger in
Thermal camera array (LWIR)	8 FLIR A68 thermal cameras	640 × 480 px at 30 FPS	LWIR (8-14 µm); 16-bit radiometric output; GigE interface; PTP sync; sync in/out, trigger in

Temporal Synchronization

Accurate synchronization is essential for coherent multi-sensor data capture. The HAL system uses a master–slave architecture, with thermal cameras acting as the master source distributing sync signals to both MOVE4D and RGB systems. A hybrid synchronization strategy, combining Precision Time Protocol (PTP) and hardware triggers, achieves high-precision inter-device synchronization, enabling reliable frame-by-frame analysis.

Spatial Calibration of Subsystems

To enable data fusion, all sensors share a common spatial reference frame obtained through a multi-step calibration process that aligns MOVE4D point clouds, RGB images, and thermal data via extrinsic transformations.
Three calibration tools are employed: (i) an **optical wand** with active spherical markers (IR+green) for MOVE4D–RGB calibration and alignment; (ii) a **thermal wand** with emissive markers for thermal camera calibration; and (iii) a **combined reference object** with both optical and high-emissivity markers to define a common spatial frame.

The procedure was conducted in two stages:

Stage 1: MOVE4D–RGB Calibration. The RGB cameras were aligned to the MOVE4D system using the optical wand (Figure 4), whose three fixed markers were tracked across ≥500 frames to solve for intrinsic and extrinsic parameters. The coordinate system was defined via an L-shaped blackbody reference board embedding both optical and thermal markers. This stage yielded rigid transformation matrices that mapped the RGB system into the MOVE4D 3D coordinate space.

Stage 2: MOVE4D–Thermal Calibration. Thermal cameras were calibrated using the thermal wand and aligned to the common frame established in Stage 1 via the combined reference object. The known spatial rela- tionship between high-emissivity and optical markers allows sub-millimeter registration of all modalities within a shared coordinate system. This enables pixel-wise projection of 2D temperature data onto 3D surfaces ensuring anatomical precision.

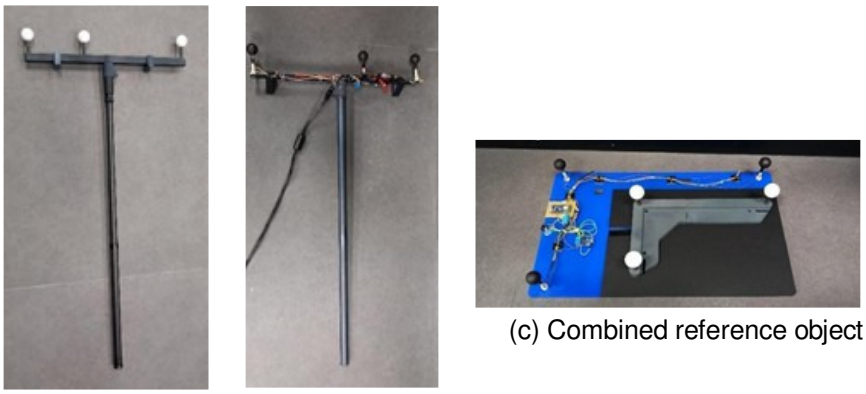

(a) Optical wand (b) Thermal wand (c) Combined reference object

Figure 4: (a) Optical wand for MOVE4D–RGB calibration (40 cm marker spacing), (b) Thermal wand for thermal camera calibration; (c) Combined reference object integrating high-emissivity markers and optical markers.

3.2.2. Gold Standard References

Although FITME prioritizes radiation-free assessment, two reference imaging methods were included to provide ground-truth data:

Dual-Energy X-ray Absorptiometry (DXA): The clinical gold standard for total and regional composition [24, 30], providing precise estimates of fat mass, lean tissue, and bone mineral content across body segments. Radiation exposure is minimal (≈0.0016 mSv, less than one day of natural background).

Low-Dose Computed Tomography (CT): Used for visceral (VAT) and subcutaneous (SAT) adipose quantification [5, 24]. A custom low-dose protocol reduced exposure by ∼90% (effective dose 2.4–3.0 mSv vs. 24–27 mSv in conventional CT). Segmentation using 3D Slicer yielded volumetric and mass measures for adipose tissue (threshold: –205 to –51 HU).

3.3. Dataset

With the HAL system fully integrated and spatiotemporally calibrated, each participant generates synchronized data streams: (i) dense 3D point clouds and post-processed meshes (morphology), (ii) high-resolution RGB recordings (motion and texture), and (iii) thermal maps (skin temperature). This synchronized acquisition enables identification of subtle physiological patterns, such as muscle activation through localized thermal variations during motion with precise anatomical co-registration (Figure 3). From these reconstructions, anthropometric indices, shape descriptors, kinematic parameters, and thermal indicators are derived and combined into composite Obesity Indicators (OIs)

(Figure 5).
Beyond HAL acquisitions, the FITME dataset integrates complementary modalities to enrich and validate predictive AI models. Details of the dataset's output structure are summarized in Appendix A (Table 2).

3.4. AI-Driven Radiation-Free Predictive Models

To fully leverage the multi-sensor data, FITME develops AI-based predictive models integrating information across all domains. Separate models are initially trained using: (i) morphofunctional and thermal features (3D shape, motion, thermographic patterns), and (ii) Supplemental Biological Indicators (S-BIs) encompassing genetic, biochemical, and microbiota data. These data streams, along with sociodemographic variables, are subsequently fused into a unified AI framework for MetS risk prediction.

Models are validated against gold-standard modalities, quantifying the accuracy of non-invasive, radiation-free estimations. This process also generates a robust training dataset for machine learning, enabling progressive inference of internal body composition from external data alone. By employing feature-level fusion and cross-domain learning, the FITME framework enhances the robustness and generalizability of predictive models, transforming heterogeneous health data into personalized obesity profiles.
As shown in Figure 5, the pipeline merges external radiation-free data sources—morphofunctional (3D/4D scanning, IRT, motion, dynamometry) with S-BIs and sociodemographic data to derive OIs used for model train- ing. From these OIs, AI-driven radiation-free models are trained capable of predicting body composition, shape, muscular function, and ultimately MetS risk.

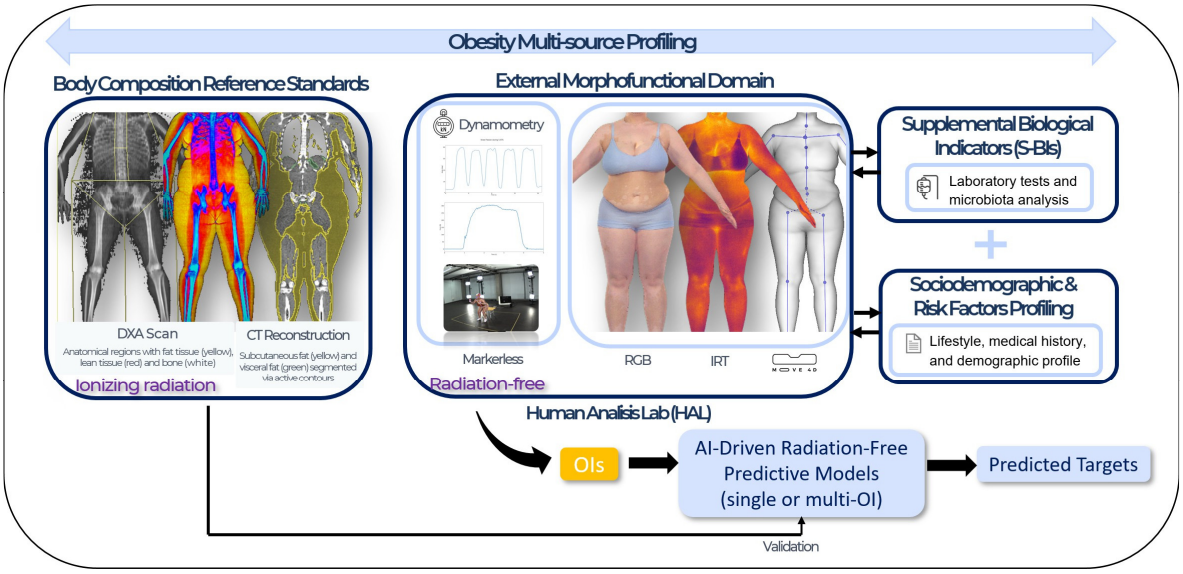

Figure 5: Schematic overview of the FITME framework: integration of multiple data domains to train AI models predicting obesity-related outcomes from composite, radiation-free Obesity Indicators (OIs).

4. Results

4.1. Case Study: High-Risk Obesity Profile

Participant profile. The representative case involves a 50-year-old woman (height 1.58 m, weight 82.1 kg; BMI=32.9 kg/m^2) with class I obesity and no major comorbidities at baseline. She completed the full FITME assessment to characterize her individualized obesity profile.

Morphological and anthropometric Analysis

A standardized whole-body 3D scan in A-pose was performed, generating a high-fidelity digital avatar from which circumferences, volumes, and body-shape indices were automatically extracted (Figure 6).

Analysis revealed a predominantly central adiposity pattern (android type), with a waist circumference of ~106 cm, exceeding the 88 cm risk threshold for women [8, 30]. The 3D-derived waist-to-hip ratio (WHR) was 0.91

(cutoff >0.85 for women [31]), and the waist-to-height ratio (WHtR) was 0.67, above the 0.5 benchmark for cardiometabolic risk [32]. These parameters confirm an android obesity phenotype (apple-shaped body type), historically linked to visceral fat accumulation and increased cardiometabolic risk [31]. These radiation-free morphological ratios serve as practical surrogates for visceral adiposity and validate the use of 3D anthropometric

markers for metabolic risk evaluation. The torso accounted for ~60% of total body volume, compared to ~27% in the legs, producing a trunk-to-leg ratio of ~2.2:1, corresponding to the metric introduced by Wilson et al. (2013) [33], which has been associated with increased diabetes and mortality risk. The 3D model revealed anterior abdominal protrusion and mild lumbar lordosis, likely reflecting postural adaptations to excess abdominal mass. These morphological descriptors can serve as radiation-free indicators of subcutaneous fat distribution, particularly when integrated with thermal maps and anatomical landmarks for personalized health avatars.

Dynamic 4D acquisitions produced watertight mesh sequences capturing simultaneous posture and motion. Analysis revealed notable soft-tissue displacement in the torso: waist circumference fluctuated by ~2.5% (2–3 cm) during squats and jumps, and chest surface area varied by ~5% through the bounce cycle. These oscillations illustrate how soft tissues store and release energy during vertical motion, a phenomenon amplified by the elevated trunk-to-leg volume ratio. Despite this, no significant lateral asymmetry was observed during landings. Overall, 4D scanning enhanced static anthropometry by showing abdominal mass distribution during motion [27].

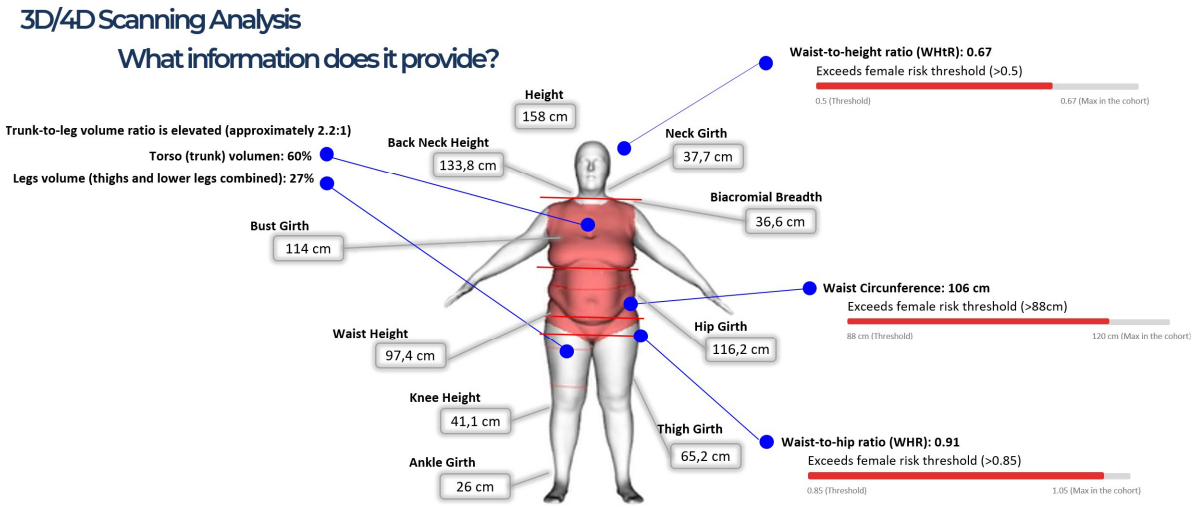

Figure 6: MOVE4D 3D body avatar enabling automatic extraction of anthropometric indices.

DXA Body Composition

DXA analysis showed: (i) total mass of 82.1 kg, (ii) 37.2 kg of fat mass (46.3%), (iii) 43.1 kg lean mass, and (iv) 2.3 kg bone mineral content. These results confirm severe adiposity with a near 1:1 fat-to-lean ratio (DXA obesity threshold >35% for women [34]). Fat distribution was predominantly central (android/gynoid ratio = 0.98), and VAT area ~200 cm^2, exceeding the 100 cm^2 risk threshold. Lean mass index (ALMI = 6.4 kg/m^2), was above the sarcopenia cutoff (5.5 kg/m^2) [35, 36], but slightly below the mean for women of comparable BMI. These measures provided reference data for model calibration and validation.

CT Low-Dose Protocol

Low-dose CT confirmed marked VAT accumulation: VAT volume was 4,088 cm^3 (≈4.1 L, 3.68 kg assuming 0.9 kg/L fat density). SAT volume was 39,615 cm^3 (≈39.6 L, 35.7 kg). VAT/SAT ratio was 0.43, surpassing the >0.4 cutoff proposed by Ryo et al. (2014) [5] for visceral obesity. CT-derived ground-truth values corroborated DXA estimates and provided detailed internal fat maps for model validation.

Thermography and Metabolic Activity

Temperature measurements were recorded before (PRE) and after (POST) cold exposure testing. High-sensitivity FLIR A68 IRT cameras (<50 mK), captured subtle surface temperature variations and asymmetries. Results showed: (i) tympanic temperature: +0.2 °C increase (ThermoScan LF20), (ii) forehead: +0.9 °C, and (iii) left waist: +0.84 °C indicating localized vasodilation and metabolic activation in response to cold exposure. In con- trast, decreases were noted in: (i) ear (–2.52 °C), (ii) feet (–1.82 °C), and (iii) left hamstring (–1.42 °C).

These spatially specific changes (detailed in Appendix B, Table 3) suggest reduced peripheral circulation and heat dissipation. The participant exhibited characteristics of a “chilly thermotype” [37], demonstrating discomfort at temperatures slightly below thermoneutrality. Cooler abdominal regions were consistent with the insulating effect of subcutaneous fat, while mild warmth around the neck and upper back indicated compensatory heat retention. No abnormal focal “hot spots” indicative of inflammation were detected.

IRT thus provides a functional and non-invasive layer to body composition analysis, offering fine-grained, radiation-free insights into thermoregulation and metabolic status, serving as a practical complement to PET imaging [23].

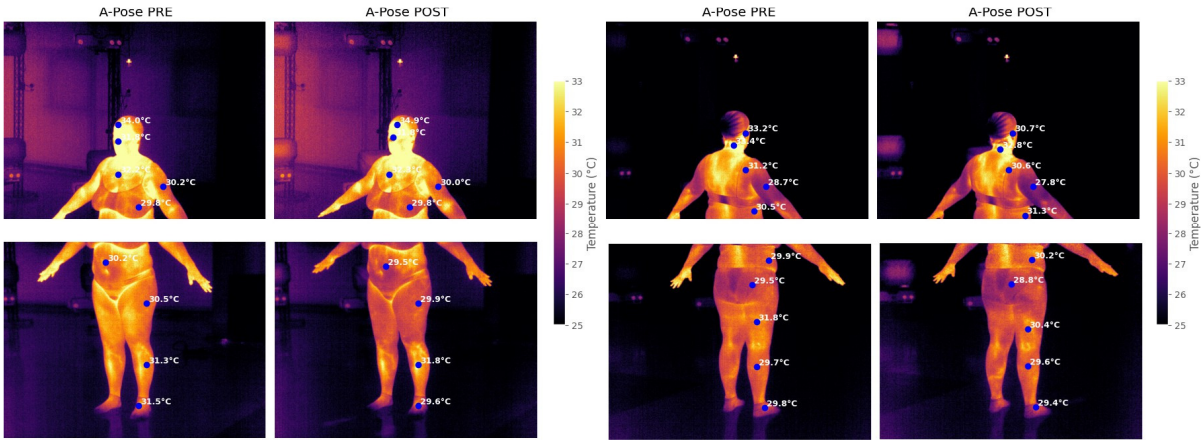

Figure 7: High-resolution IRT images before (PRE) and after (POST) testing.

Bioimpedance

Single-frequency BIA estimated ~42% body fat, slightly below the DXA result. Total body water was ~36 L (44% of body weight), consistent with high fat mass (since adipose tissue contains less water). Multi-frequency BIA indicated normal hydration but a low phase angle, reflecting reduced cellular integrity.

Biomechanical and Markerless Motion Analysis

Gait analysis revealed: (i) stride length: 1.17 m (shortened), and (ii) cadence: 120 steps/min (elevated). This combination reflects a compensatory strategy to maintain speed and stability. The five-times sit-to-stand (5×STS) test took 17.3 s, exceeding the healthy reference range (≤12–15 s), indicating reduced lower-limb strength and endurance. Phase-specific data showed slower transitions (stand-up ~1.4 s; descent ~2.1 s) and a left-sided asymmetry, suggesting preferential load-bearing. All repetitions were completed pain-free, confirming functional independence but subtle mobility limitations. Grip strength (17.5–17.8 kg) was low but within normative values for age and sex. Quadriceps force reached ~32.5 kg, below the normative 40–45 kg range for women [38, 39]. Quadriceps strength is a sensitive marker of functional decline in obesity [38,40]. Combined with excess adiposity, this profile indicates greater joint stress, higher movement cost, and increased disability risk [39, 40].

Supplemental Biological Indicators (S-BIs)

S-BIs analysis revealed early-stage metabolic dysregulation, with dyslipidemia (high triglycerides, low HDL) and borderline fasting glucose. Integration of these biochemical and molecular profiles with radiation-free data provides a key foundation for developing robust, individualized predictive models of MetS risk [4].

5. Conclusion

The integration of 3D/4D body scanning, functional analysis, and IRT within the HAL, enables an extensive char- acterization of obesity that surpasses conventional methods. This multi-sensor, radiation-free system produces a rich, anatomically coherent dataset suitable for AI-based modeling, capturing inter-individual variability among subjects. The radiation-free modalities are rigorously validated against gold-standard references (DXA/CT) to ensure accuracy and reproducibility. The resulting dataset underpins the training of AI algorithms to infer inter- nal composition, morphology, and muscular function solely from external optical and thermal Obesity Indicators (OIs). When further integrated with sociodemographic data and S-BIs, the FITME framework supports the cre- ation of advanced predictive models for MetS risk estimation.

Once validated across the full cohort of 100 participants, this framework has the potential to evolve into a routine clinical pathway, enabling radiation-free, precision health assessment. By linking external morphology, internal composition, and molecular biomarkers, FITME establishes validated reference data for algorithm training and clinical translation. Ultimately, the project will demonstrate how digital health technologies can decouple accurate obesity assessment from ionizing radiation, accelerating the transition toward precision and personalized medicine, aligning directly with the mission of the 3DBody.Tech community to leverage digital innovation for personalized health.

Appendix A. FITME Multi-source Dataset

Table 2: Summary of multi-source output data from the FITME pipeline.

Data Source	Data Type	Output data (file format)	Description
MOVE4D capture system	3D Anthropometry and body geometry	3D meshes (.ply, .obj), point clouds (.ply), circumferences, volumes, body shape indices (.csv)	Generates hundreds of standardized anthropometric variables including heights, lengths, circumferences, widths and depths, as well as segmented body volumes (full body, torso, limbs) and surface areas. Provides static measures and dynamic 4D motion sequences with posture and soft-tissue deformation.
3D Avatar Body App	Body shape morphology and anthropometric reporting	3D avatar files (.obj, .ply, .fbx), anthropometric datasets (.csv, .xlsx)	Generates high-resolution digital avatars and standardized anthropometric measurements. Provides visual feedback while supporting morphology data analysis.
RGB Multi-camera array	Markerless motion kinematics	Raw frames (.raw), video streams (.avi, .mp4), frame sequences (.png), kinematic variables (.csv, .xlsx)	Computer vision algorithms track posture and joint trajectories during gait and 5STS.
Thermal camera array	Skin Temperature and Thermographic patterns	Thermal captures (.flircapt), raw frames (.raw), calibrated images (.png, .tiff), thermal maps (.csv)	Provides high-resolution skin temperature maps, capturing regional variations and asymmetries as indicators of thermoregulation, vascular function, or local inflammation. Safe, contact-free, and non-invasive alternative to traditional imaging.
DXA Imaging	Body composition	Scan outputs (.bmp), composition reports (.pdf, .csv)	Gold standard for regional composition and adipose tissue, used as reference for model validation.
CT Imaging (low-dose)	Visceral and subcutaneous fat segmentation	CT slices (.dcm), segmentation report (.pdf), segmented 3D volumes (.nii), 3D surfaces (.stl)	Gold-standard reference quantifying adipose tissue; provides 3D anatomical fat maps. Reference for validating non-invasive modalities.
Bioimpedane (BIA)	Body composition and hydration	Raw data and summary tables (.csv, .xlsx)	Rapid, non-invasive estimates of adiposity and hydration, complementary to DXA/CT.
Dynamomety	Muscle strength	Force curves (.csv), sum marymetrics (.xlsx)	Portable tests of upper- and lower- limb strength (grip strength, quadriceps force). Functional insight.
Laboratory tests	Clinical biomarkers	Results (.pdf, .csv)	Selected blood biochemistry variables.
Genetic and microbiota profiling	Molecular signatures	Processed data (.csv, .xlsx)	Omics-based phenotyping to detect inter-individual variability and stratify obesity subtypes.
Sociodemographic and question-naires	Lifestyle, medical history, and demographic profile	Responses (.xlsx, .csv, .pdf)	Includes age, sex, education, occupation, civil status, lifestyle habits, diet, medication use, and self-reported chronic conditions. Provides essential contextual data for stratifying participants and interpreting multiparametric results.

Appendix B. Example of Thermal Responses at Anatomical Landmarks

Table 3: Thermal responses at selected anatomical landmarks before (PRE) and after (POST) testing, showing temperature differences (∆T).

Landmark	Cam #	PRE (°C)	POST (°C)	∆*T* (°C)
Tympanic thermometer	-	35.7	35.9	+0.2
Forehead	4	34.04	34.94	+0.9
Nose	4	31.76	31.60	-0.16
Ear	8	33.18	30.66	-2.52
Nape	8	33.37	32.80	-0.57
Chest	4	32.17	32.28	+0.11
Right shoulder blade	8	31.22	30.63	-0.59
Left breast (bra)	4	29.78	29.76	-0.02
Left arm (front)	4	30.18	30.03	-0.15
Right arm (back)	8	28.68	27.80	-0.88
Left waist side	8	30.49	31.33	+0.84
Left lower back	7	29.87	30.25	+0.38
Abdomen	3	30.21	29.54	-0.67
Right buttock	7	29.49	28.83	-0.66
Right thigh	3	30.46	29.93	-0.53
Left hamstring	7	31.82	30.40	-1.42
Right leg shin	3	31.34	31.81	+0.47
Left calf	7	29.72	29.63	-0.09
Instep	3	31.46	29.64	-1.82
Left foot (sock)	7	29.85	29.44	-0.41

References

[1] Sweatt, Katherine et al. “Strengths and Limitations of BMI in the Diagnosis of Obesity: What is the Path Forward?.” Current obesity reports vol. 13,3 (2024): 584-595. doi:10.1007/s13679-024-00580-1

[2] S. B. Heymsfield, C. B. Ebbeling, J. Zheng, A. Pietrobelli, B. J. Strauss, A. M. Silva, and D. S. Ludwig, ”Multi-component molecular-level body composition reference methods: evolving concepts and future direc- tions,” *Obesity Reviews*, vol. 16, no. 4, pp. 282–294, 2015, doi: 10.1111/obr.12261.

[3] World Health Organization, “Obesity and overweight: Key facts,” *WHO Fact Sheet*, Geneva, 2024. [Online]. Available: https://www.who.int/news-room/fact-sheets/detail/ obesity-and-overweight

[4] K. Watanabe, T. Wilmanski, C. Diener, et al., ”Multiomic signatures of body mass index identify heteroge- neous health phenotypes and responses to a lifestyle intervention,” *Nature Medicine*, vol. 29, pp. 996–1008, 2023, doi: 10.1038/s41591-023-02248-0.

[5] M. Ryo, et al., ”Clinical significance of visceral adiposity assessed by computed tomography: A Japanese perspective,” *World Journal of Radiology*, vol. 6, no. 7, pp. 409–416, 2014, doi: 10.4329/wjr.v6.i7.409.

[6] J. Guo, et al., ”Infrared thermography-based radiomics for early detection of metabolic syndrome,” *Scientific Reports*, vol. 15, no. 1, p. 13984, 2025, doi: 10.1038/s41598-025-98831-1.

[7] Y. Sun, X. Lin, Z. Zou, et al., ”Association between visceral fat area and metabolic syndrome in individuals with normal body weight: insights from a Chinese health screening dataset,” *Lipids in Health and Disease*, vol. 24, p. 57, 2025, doi: 10.1186/s12944-025-02482-0.

[8] World Health Organization, *Waist Circumference and Waist–Hip Ratio: Report of a WHO Expert Consul- tation*, Geneva: WHO, Dec. 2008. [Online]. Available: https://apps.who.int/iris/handle/10665/44583

[9] T. Lobstein, "Obesity prevention and the global syndemic: Challenges and opportunities for the World Obesity Federation," *Obesity Reviews*, vol. 20, pp. 6–9, 2019, doi:10.1111/obr.12888.

[10] A. Afshin, M. H. Forouzanfar, M. B. Reitsma, et al., "Health effects of overweight and obesity in 195 coun- tries over 25 years," *New England Journal of Medicine*, vol. 377, no. 1, pp. 13–27, 2017, doi: 10.1056/NEJ- Moa1614362.

[11] A. Galassi, K. Reynolds, and J. He, "Metabolic syndrome and risk of cardiovascular disease: A meta-analysis," *American Journal of Medicine*, vol. 119, no. 10, pp. 812–819, 2006, doi: 10.1016/j.amjmed.2006.02.031.

[12] S. M. Grundy, H. B. Brewer, J. I. Cleeman, S. C. Smith, and C. Lenfant, "Definition of metabolic syndrome: Report of the National Heart, Lung, and Blood Institute/American Heart Association conference on scientific issues related to definition," *Circulation*, vol. 112, no. 17, pp. 2735–2752, 2005, doi: 10.1161/CIRCULA- TIONAHA.105.169404.

[13] K. G. Alberti, R. H. Eckel, S. M. Grundy, et al., "Harmonizing the metabolic syndrome: A joint interim state- ment...," *Circulation*, vol. 120, no. 16, pp. 1640–1645, 2009, doi:10.1161/CIRCULATIONAHA.109.192644

[14] D. M. Boudreau, P. A. Malone, and M. Raebel, "Health care utilization and costs by metabolic syn- drome risk factors," *Metabolic Syndrome and Related Disorders*, vol. 7, no. 4, pp. 305–314, 2009, doi: 10.1089/met.2008.0070.

[15] A. Romero-Corral, V. K. Somers, J. Sierra-Johnson, et al., "Normal weight obesity: a risk factor for cardiometabolic dysregulation and cardiovascular mortality," *European Heart Journal*, vol. 31, no. 6, pp. 737–746, 2008, doi: 10.1093/eurheartj/ehp487.

[16] M. Wang, et al., "Utilizing Anthropometric Measurements and 3D Scanning for Health Assessment in Clin- ical Practice," *Physical Activity and Health*, vol. 8, no. 1, pp. 182–196, 2024, doi: 10.5334/paah.379.

[17] M. Gao, et al., "An exploration of new methods for metabolic syndrome examination by infrared thermog- raphy and knowledge mining," *Scientific Reports*, vol. 12, p. 6377, 2022, doi: 10.1038/s41598-022-10422-6.

[18] N. G. Norgan, "Laboratory and field measurements of body composition," *Public Health Nutrition*, vol. 8, no. 7A, pp. 1108–1122, 2005, doi: 10.1079/phn2005799.

[19] F. X. Pi-Sunyer, "The medical risks of obesity," *Postgraduate Medicine*, vol. 121, no. 6, pp. 21–33, 2009, doi: 10.3810/pgm.2009.11.2074.

[20] D. L. Duren, et al., "Body composition methods: comparisons and interpretation," *Journal of Diabetes Science and Technology*, vol. 2, no. 6, pp. 1139–1146, 2008, doi: 10.1177/193229680800200623.

[21] J. P. Bennett et al., "Three-dimensional optical body shape and features improve prediction of metabolic disease risk in a diverse sample of adults," *Obesity (Silver Spring)*, vol. 30, no. 8, pp. 1589–1598, 2022, doi: 10.1002/oby.23470.

[22] L. T. Leong, M. C. Wong, Y. E. Liu, et al., "Generative deep learning furthers the understanding of local distributions of fat and muscle on body shape and health using 3D surface scans," *Communications Medicine*, vol. 4, p. 13, 2024, doi: 10.1038/s43856-024-00434-w.

[23] S. H. Tay, H. J. Goh, P. Govindharajulu, J. Cheng, S. G. Camps, S. Haldar, S. S. Velan, L. Sun, Y. Li,

C. J. Henry, and M. K. Leow, "Brown fat activity determined by infrared thermography and thermogenesis measurement using whole body calorimetry (BRIGHT Study)," *Physiological Research*, vol. 69, no. 1, pp. 85–97, Feb. 2020, doi: 10.33549/physiolres.934190.

[24] S. Jeon, M. Kim, J. Yoon, S. Lee, and S. Youm, "Machine learning-based obesity classification considering 3D body scanner measurements," *Scientific Reports*, vol. 13, no. 1, p. 3299, 2023, doi: 10.1038/s41598-023- 30434-0.

[25] S. Scataglini, E. Abts, C. Van Bocxlaer, M. Van den Bussche, S. Meletani, and S. Truijen, "Accuracy, validity, and reliability of markerless camera-based 3D motion capture systems versus marker-based 3D motion capture systems in gait analysis: A systematic review and meta-analysis," *Sensors*, vol. 24, no. 11, p. 3686, Jun. 2024, doi: 10.3390/s24113686.

[26] R. Heuberger, P. Kinnicutt, and T. Domina, "The relationship between thermal imaging and waist circumfer- ence in young adults," *Health*, vol. 4, no. 12A, pp. 1485–1491, 2012, doi: 10.4236/health.2012.412A213.

[27] K. Bartol, D. Bojanic´, T. Petkovic´, and T. Pribanic´, "A review of body measurement using 3D scanning," *University of Zagreb, Faculty of Electrical Engineering and Computing, Dept. of Electronic Systems and Information Processing*, Croatian Science Foundation, Project IP-2018-01-8118, 2020.

[28] MOVE 4D Project, "High-speed multimodal 4D body capture," [Online]. Available: https://www.move4d.net/#:~:text=HIGH. [Accessed: Sep. 3, 2025].

[29] E. Parrilla Bernabe´, A. Ballester, F. Parra, A. V. Ruescas, J. Uriel, D. Garrido, and S. Alemany, "MOVE 4D: Accurate High-Speed 3D Body Models in Motion," in *Proc. of the 10th Int. Conf. on 3D Body Scanning and Processing Technologies*, vol. 10, pp. 30–34, 2019, doi: 10.15221/19.030.

[30] D. A. Levine, V. Calhoun, D. A. Howard, et al., "Moderate waist circumference and hypertension preva- lence: the REGARDS Study," *American Journal of Hypertension*, vol. 24, no. 4, pp. 482–488, 2011, doi: 10.1038/ajh.2010.258.

[31] R. Ross, I. J. Neeland, S. Yamashita, et al., "Waist circumference as a vital sign in clinical practice: a Consen- sus Statement from the IAS and ICCR Working Group on Visceral Obesity," *Nature Reviews Endocrinology*, vol. 16, pp. 177–189, 2020, doi: 10.1038/s41574-019-0310-7.

[32] S. Gibson and M. Ashwell, "A simple cut-off for waist-to-height ratio (0.5) can act as an indicator for cardiometabolic risk: recent data from adults in the Health Survey for England," *British Journal of Nutrition*, vol. 123, no. 6, pp. 681–690, 2020, doi: 10.1017/S0007114519003301.

[33] J. P. Wilson, A. M. Kanaya, B. Fan, and J. A. Shepherd, "Ratio of trunk to leg volume as a new body shape metric for diabetes and mortality," *PLOS ONE*, vol. 8, no. 7, e68716, 2013, doi: 10.1371/jour- nal.pone.0068716.

[34] J. A. Pasco, K. L. Holloway, A. G. Dobbins, M. A. Kotowicz, L. J. Williams, and S. L. Brennan, "Body mass index and measures of body fat for defining obesity and underweight: a cross-sectional, population-based study," *BMC Obesity*, vol. 1, p. 9, Jun. 2014, doi: 10.1186/2052-9538-1-9.

[35] R. N. Baumgartner, K. M. Koehler, D. Gallagher, L. Romero, S. B. Heymsfield, R. R. Ross, P. J. Garry, and R. D. Lindeman, "Epidemiology of sarcopenia among the elderly in New Mexico," *American Journal of Epidemiology*, vol. 147, no. 8, pp. 755–763, 1998, doi: 10.1093/oxfordjournals.aje.a009520.

[36] A. J. Cruz-Jentoft, G. Bahat, J. Bauer, et al., "Sarcopenia: revised European consensus on definition and diagnosis," *Age and Ageing*, vol. 48, no. 1, pp. 16–31, 2019, doi: 10.1093/ageing/afy169.

[37] R. Latorre-Sa´nchez, et al., "Digital human updated: Merging the thermal layers with the 3D anthropometric model," in *Digital Human Modeling and Applications in Health, Safety, Ergonomics and Risk Management. Human Body, Motion and Behavior*, Springer, Cham, pp. 541–552, 2019, doi: 10.1007/978-3-030-20216- 3 48.

[38] R. McGrath, et al., "The association of quadriceps strength with mobility in older adults: A systematic re- view," *Journal of Cachexia, Sarcopenia and Muscle*, vol. 13, no. 1, pp. 42–56, 2022, doi: 10.1002/jcsm.12840.

[39] M. Zamboni, et al., "Sarcopenic obesity: a new category of obesity in the elderly," *Nutrition, Metabolism and Cardiovascular Diseases*, vol. 18, no. 5, pp. 388–395, 2008, doi: 10.1016/j.numecd.2007.10.002.

[40] E. Roh and K. M. Choi, "Health consequences of sarcopenic obesity: A narrative review," *Frontiers in Endocrinology*, vol. 11, p. 332, 2020, doi: 10.3389/fendo.2020.00332.